
The Dynamics of SQUIDs and Coupled Pendula

Don G Aronson and Hans G Othmer

¹ School of Mathematics and Institute for Mathematics and Its Applications,
University of Minnesota, Minneapolis, USA

² School of Mathematics and Digital Technology Center, University of Minnesota,
Minneapolis, USA

Josephson [8] predicted in 1962 that a DC tunnel current would flow between two superconductors connected by a thin insulating layer of thickness less than about 20 \AA in the absence of a voltage difference, an effect now called the DC Josephson effect. The quantum-mechanical current, called the superconducting current, arises from the tunneling of Cooper pairs of electrons of opposite spin and momenta and is given by

$$I_s = I_c \sin \phi, \quad (1)$$

where I_c is the critical current and ϕ is the difference of the phases of the wave functions of the two superconductors. This gives the ideal current through a junction, but in real circuits there are resistive and capacitive currents as well. One of the standard models of a more realistic circuit is the so-called Stewart-McCumber resistively-shunted-junction (or RSJ) model, which is described by the following equation for the current [6, 9]:

$$\frac{hC}{2e} \frac{d^2 \phi}{dt^2} + \frac{h}{2eR} \frac{d\phi}{dt} + I_c \sin \phi = I. \quad (2)$$

Here, h is Planck's constant, e is the charge on an electron, $h/2e$ is the flux quantum, C is the capacitance, R is the resistance, and I is the imposed bias current. To simplify (2) define the frequency $\Omega = \sqrt{2eI_c/hC}$ and the scaled time $\tau = \Omega t$; then (2) becomes

$$\ddot{\phi} + \varepsilon \dot{\phi} + \sin \phi = i, \quad (3)$$

where $\varepsilon = (\Omega RC)^{-1}$, $i = I/I_c$, and the dot denotes derivation with respect to the rescaled time τ .

A very useful correspondence of this system to a pendulum provides insight into the dynamics studied later. In fact, the pendulum will serve as the basic physical model; see also [1]. Suppose that a pendulum consists of a bob of

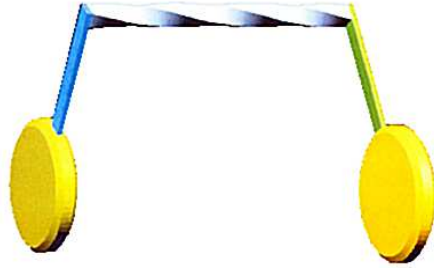


Fig. 1. Two pendula coupled via a torsion bar. From D.G. Aronson, E.J. Doedel and H.G. Othmer, The dynamics of coupled current-biased Josephson junctions II, *Internat. J. Bifur. Chaos Appl. Sci. Engrg.* 1(1) (1991) 51–66 ©1991 by World Scientific Publishers; reprinted with permission.

mass m that is attached to a (weightless) rod of length L . Then the equation of motion is

$$\Lambda \frac{d^2\phi}{dt^2} + \eta \frac{d\phi}{dt} + mgL \sin \phi = T, \quad (4)$$

where $\Lambda = mL^2$ is the moment of inertia of the pendulum, g is the gravitational acceleration, η is the damping, ϕ is the angle between the bob and vertical measured from the downward position, and T is the applied torque. After non-dimensionalization this leads to (3).

When a ring of superconducting material contains two Josephson junctions, the result is a superconducting quantum interference device (SQUID), so called because the wave functions of the Cooper pairs at each junction interfere. SQUIDS are among the most sensitive devices for detecting magnetic fields — a SQUID is capable of detecting magnetic fields of around 2 picotesla, i.e., at the quantum flux level. The coupling between phases across the junctions is proportional to the difference of phases, and therefore, the system of equations governing a SQUID is

$$\begin{cases} \ddot{\phi}_1 + \varepsilon \dot{\phi}_1 + \sin \phi_1 = \gamma(\phi_2 - \phi_1) + I, \\ \ddot{\phi}_2 + \varepsilon \dot{\phi}_2 + \sin \phi_2 = \gamma(\phi_1 - \phi_2) + I. \end{cases} \quad (5)$$

Here, γ is the coupling coefficient, and the dimensionless bias current I is assumed to be the same for both junctions.

An identical pair of equations governs the motion of two pendula coupled by a linear torsional spring or bar, and forced with an applied torque I ; see Fig. 1. We use this system as the paradigm in this chapter and we attempt to synthesize the results of [3, 5] and the unpublished study [2], which are all written in collaboration with Eusebius Doedel. The work involves extensive numerical studies that were carried out using DSTOOL, MatLab, and primarily, AUTO. In the next section we analyze the equilibria of (5). Section 2 considers the undamped undriven case, which is part of the unpublished results in [2]. We analyze both equilibria and periodic orbits for this case, and

also discuss the computation of heteroclinic connections. Finally, Sec. 3 shows the existence of so-called rotations, periodic solutions with a period this is an integer multiple of the forcing frequency. We discuss their stability in Sec. 4 and draw some conclusions in Sec. 5.

1 Equilibria and their stability

We begin by analyzing the existence and stability of equilibria for the coupled system. Clearly (5) is invariant under the transformation $\phi_i \rightarrow \phi_i + 2\pi$ and, thus, defines a flow on the product space $\{\mathbb{S}^1 \times \mathbb{R}\}^2$. In addition, (5) is invariant under the transformations $\phi_i \rightarrow \phi_{i+1} \pmod{2}$ and $(\phi_i, I) \rightarrow (-\phi_i, -I)$. Therefore, we assume that $I \geq 0$ from now on. In order to analyze (5) it is convenient to introduce the variables

$$r = \frac{1}{2}(\phi_1 - \phi_2) \quad \text{and} \quad s = \frac{1}{2}(\phi_1 + \phi_2),$$

where r is (half) the instantaneous phase difference and s is the average phase difference. In these variables, and when written as a first-order system, (5) becomes

$$\begin{cases} \dot{r} = u, \\ \dot{s} = v, \\ \dot{u} = -\varepsilon u - \sin r \cos s - 2\gamma r, \\ \dot{v} = -\varepsilon v - \cos r \sin s + I. \end{cases} \quad (6)$$

If $\gamma = 0$ then the pendula are uncoupled, and if $r = 0$ then they are in phase or synchronized. The subspace $r = u = 0$ is invariant under the flow associated with this system and we refer to it as the *in-phase subspace*. The dynamics on this subspace are well characterized, even when the forcing is time dependent, because the fourth-order system reduces to a second-order system [4, 13].

The equilibria of (6) are given by $(R, S, 0, 0)$, where R and S are solutions to the system

$$\begin{cases} \sin R \cos S = -2\gamma R, \\ \cos R \sin S = I. \end{cases} \quad (7)$$

Solutions with $|R| > 0$ are called asynchronous equilibria, and those with $R = 0$ are called synchronous equilibria. Clearly the existence of equilibria is independent of the damping, but the forcing must be small enough ($|I| < 1$) to have an equilibrium. In the SQUID context this means that the bias current must be smaller than the superconducting current. In addition, solutions must satisfy $|R| < 1/2\gamma$, and therefore the asynchronous solutions approach synchronous solutions as the coupling strength increases.

With a slight abuse of notation we use the abbreviation (R, S) for equilibria, and in this notation we have the following: for $\gamma = 0$ system (7) has two countably infinite families of equilibria $\{(R_m, S_m)\}$ and $\{(R_n, S_n)\}$ that satisfy

$$R_m = \arccos(-1)^m I, \quad S_m = \frac{2m+1}{2} \pi \quad (8)$$

and

$$R_n = n\pi, \quad S_n = (-1)^n \arcsin I, \quad (9)$$

respectively. If we define $\sigma = \arcsin I$ then the complete set of solutions to (8) is generated by 2π -translates in S and π -translates along the diagonal of the basic sets

$$(R, S) = \left(\pm \left[\frac{\pi}{2} - \sigma \right], \frac{\pi}{2} \right) \quad \text{and} \quad (R, S) = (0, \{\sigma, \pi - \sigma\}). \quad (10)$$

For example, the π -translation along the diagonal of the basic set results in the four equilibria

$$\left(\frac{3\pi}{2} - \sigma, \frac{3\pi}{2} \right), \left(\frac{\pi}{2} + \sigma, \frac{3\pi}{2} \right), (\pi, 2\pi - \sigma), \text{ and } (\pi, 2\pi + \sigma).$$

When the applied torque vanishes (7) reduces to

$$\sin R = \pm 2\gamma R. \quad (11)$$

This equation has infinitely many solutions at $\gamma = 0$, and the number of solutions decreases to zero by a sequence of saddle-node bifurcations as $|\gamma|$ increases. The last solution disappears at the value for which the line $y = \pm 2\gamma R$ is first tangent to the curve $y = \sin R$.

The local stability of any equilibrium of (6) is determined by the eigenvalues of the Jacobian of the right-hand side of (6), which is

$$J = \begin{bmatrix} 0 & 0 & 1 & 0 \\ 0 & 0 & 0 & 1 \\ -\cos R \cos S - 2\gamma & \sin R \sin S & -\varepsilon & 0 \\ \sin R \sin S & -\cos R \cos S & 0 & -\varepsilon \end{bmatrix} = \begin{bmatrix} 0 & I_2 \\ L & -\varepsilon I_2 \end{bmatrix}.$$

The eigenvalues of J are solutions to the pair of quadratic equations

$$\lambda^2 + \varepsilon\lambda - \kappa_{\pm} = 0.$$

Here κ_{\pm} are the eigenvalues of L , that is,

$$\kappa_{\pm} = \frac{1}{2} \left(\text{trace}(L) \pm \sqrt{(\text{trace}(L))^2 - 4\det(L)} \right),$$

where

$$\begin{aligned} \text{trace}(L) &= -2(\cos R \cos S + \gamma), \\ \det(L) &= (\cos R \cos S)^2 - (\sin R \sin S)^2 + 2\gamma \cos R \sin S. \end{aligned}$$

Equilibria which κ_{\pm} are both negative are stable, those with $\kappa_+ \kappa_- < 0$ have a one-dimensional stable manifold, and those for which κ_{\pm} are both positive have a two-dimensional unstable manifold.

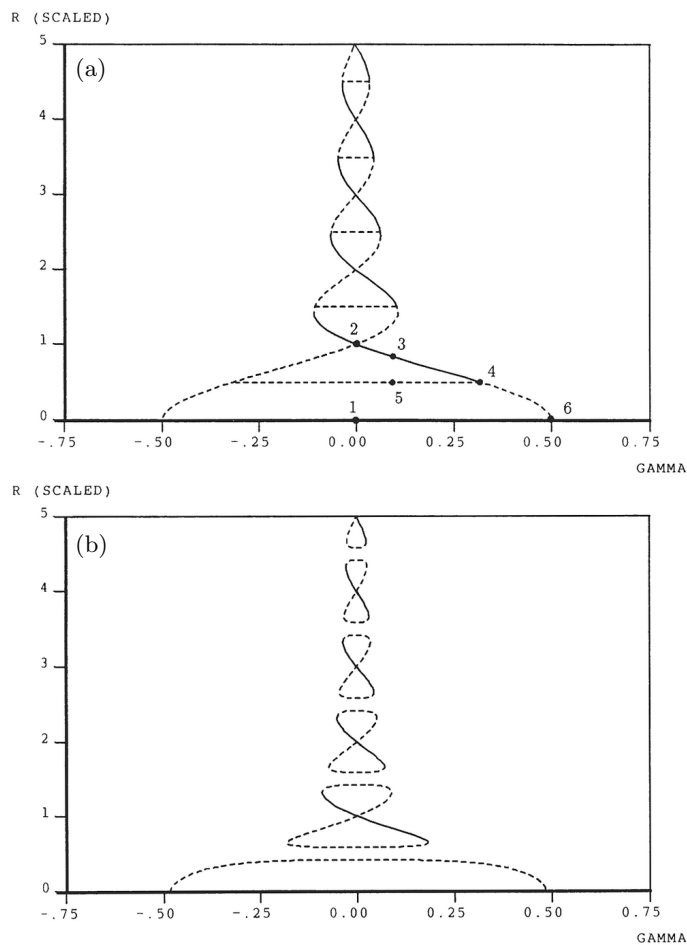


Fig. 2. The first five sets of equilibria of (6) for $\varepsilon = 0.15$ as a function of the coupling strength γ for $I = 0$ (a) and for $I = 0.25$ (b). Solid and dashed curves denote stable and unstable solutions, respectively; saddle-node bifurcations arise at the values of γ where there is a vertical tangent. From D.G. Aronson, E.J. Doedel and H.G. Othmer, The dynamics of coupled current-biased Josephson junctions II, *Internat. J. Bifur. Chaos Appl. Sci. Engrg.* 1(1) (1991) 51-66 ©1991 by World Scientific Publishers; reprinted with permission.

If $\gamma = 0$, the characteristic equation of L is

$$(\kappa + \cos R \cos S)^2 - (\sin R \sin S)^2 = 0.$$

and, therefore, for (R, S) given by (10) we have that

- $\kappa_+ = \kappa_- = -\cos \sigma < 0$ for $(R, S) = (0, \sigma)$,
- $\kappa_+ \kappa_- = -\cos^2 \sigma < 0$ for $(R, S) = (\pm(\frac{\pi}{2} - \sigma), \frac{\pi}{2})$,
- $\kappa_+ = \kappa_- = \cos \sigma > 0$ for $(R, S) = (0, \pi - \sigma)$.

Thus, of the four points, only $(R, S) = (0, \sigma)$ is stable, and the same pattern is found for all the translates of these points. In terms of the phase angles of the individual pendula, the existence and stability of equilibria at $\gamma = 0$ can be summarized as follows. The three types of solutions are:

1. solutions with $\phi_1, \phi_2 \in (0, \pi/2)$; these are asymptotically stable for any $\varepsilon > 0$.
2. solutions with $\phi_1 \in (0, \pi/2)$ and $\phi_2 \in (\pi/2, \pi)$; these have a three-dimensional stable manifold and a one-dimensional unstable manifold.
3. solutions with $\phi_1, \phi_2 \in (\pi/2, \pi)$; these have a two-dimensional stable manifold and a two-dimensional unstable manifold.

At $\gamma = 0$ there exists an infinite number of other equilibria for which $R \neq 0$, each of which can be continued for small $|\gamma|$ because none of the equilibria that exist at $\gamma = 0$ is critical in the sense that the Jacobian has one or more eigenvalues on the imaginary axis. These equilibria and their continuations are naturally grouped into families of four equilibria, as determined above, by the various choices of ϕ_1 and ϕ_2 at $\gamma = 0$. By translation in S , each of these families determine an equivalence class of families modulo 2π . For any $\gamma \neq 0$ only finitely many of these exist, the remaining ones having disappeared via saddle-node bifurcations. Each of the families contains four equilibria at $\gamma = 0$, from which the entire family can be generated by continuation. The resulting families are shown in Fig. 2(a) for zero forcing and in Fig. 2(b) for $I = 0.25$; here we plotted the phase difference R versus γ . For the n th family, $n \neq 0$, the four solutions at $\gamma = 0$ can be denoted as $(\phi_d, \phi_d - 2n\pi)$, $(\phi_u, \phi_d - 2n\pi)$, $(\phi_d, \phi_u - 2n\pi)$, and $(\phi_u, \phi_u - 2n\pi)$, where $\phi_d = \sigma$, and $\phi_u = \pi - \phi_d$; see also [5].

2 Hamiltonian dynamics

In the absence of damping and forcing (5) reduces to the Hamiltonian system

$$\begin{aligned}\ddot{\phi}_1 + \sin \phi_1 &= \gamma(\phi_2 - \phi_1), \\ \ddot{\phi}_2 + \sin \phi_2 &= \gamma(\phi_1 - \phi_2),\end{aligned}\tag{12}$$

where the energy is given by

$$\mathcal{H} = \frac{1}{2} \left(\dot{\phi}_1^2 + \dot{\phi}_2^2 \right) - (2 + \cos \phi_1 + \cos \phi_2) + \frac{\gamma}{2} (\phi_1 - \phi_2)^2.$$

In this section we summarize a portion of the results on the undamped undriven case from the unpublished work [2].

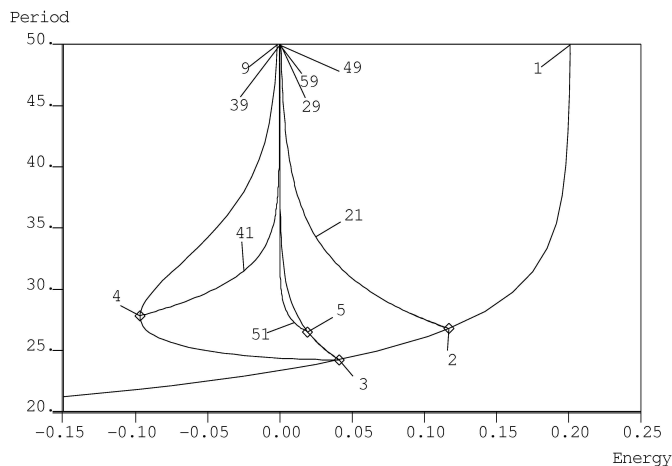


Fig. 3. The branch of antidiagonal solutions and some bifurcating branches for $\gamma = 0.01$. Where necessary, periods have been doubled to ensure that branches connect continuously.

The uncoupled system (12) with $\gamma = 0$ has equilibria at all points $e_{m,n} = (m\pi, n\pi)$ in the (ϕ_1, ϕ_2) configuration plane. In the basic square $(-\pi, \pi) \times (-\pi, \pi)$ there are heteroclinic orbits joining the diagonal points $e_{-1,-1}$ and $e_{1,1}$, the antidiagonal points $e_{1,-1}$ and $e_{-1,1}$, as well as all four pairs of neighboring corner points. The system is doubly periodic, which generates the entire plane.

For $\gamma \neq 0$ the doubly periodic structure is destroyed since the energy surfaces are bounded by the zero-velocity cylinders

$$-(2 + \cos \phi_1 + \cos \phi_2) + \frac{\gamma}{2}(\phi_1 - \phi_2)^2.$$

The symmetry that comes from translation by 2π along the diagonal remains.

When (12) is written in (r, s) variables, one sees from (6) that the diagonal $r \equiv 0$ and the antidiagonal $s \equiv 0$ are invariant. On the diagonal there are equilibria at $(k\pi, 0)$ for all integers k . These equilibria are centers for k even, while they are saddles for k odd. On the antidiagonal the equilibria are $(\rho, 0)$, where ρ is given by the solution of (11) with the negative sign. Let us suppose that there is a minimal positive solution $\rho = \rho_1$. To construct an antidiagonal solution to (6) (with $I = \varepsilon = 0$) we solve the initial value problem

$$\ddot{r} + \sin r + 2\gamma r = 0, \quad r(0) = 0 \text{ and } \dot{r}(0) = p. \tag{13}$$

The first integral for this problem is

$$\frac{1}{2}\dot{r}^2 - \cos r + \gamma r^2 = \frac{1}{2}p^2 - 1.$$

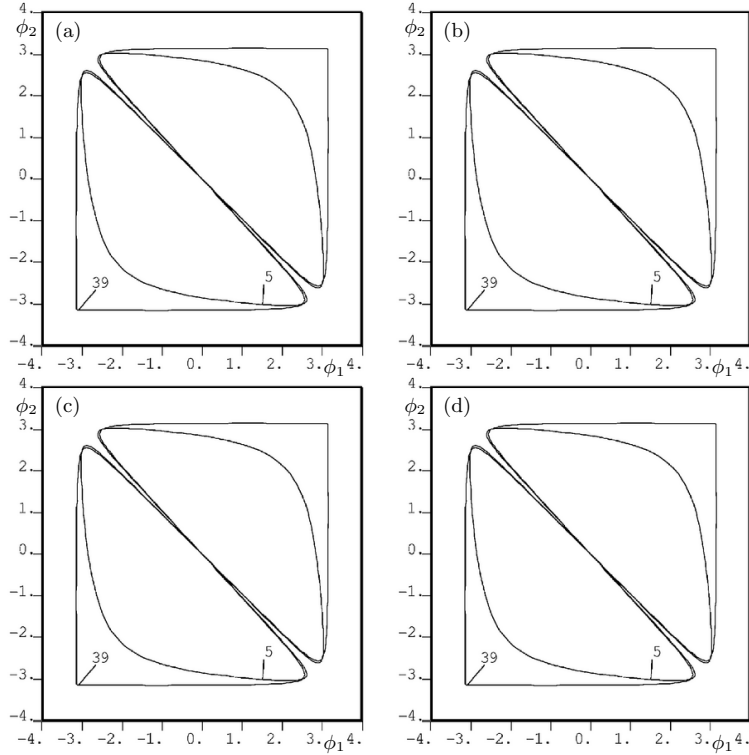


Fig. 4. The (ϕ_1, ϕ_2) component of selected solutions in Fig. 3.

The solution corresponds to a heteroclinic orbit joining the equilibria $(\pm\rho_1, 0)$ if

$$p(\rho_1) = p_1 = \sqrt{2 - 2\cos(\rho_1) + 2\gamma\rho_1^2}.$$

For $\rho < \rho_1$ the solution $p(\rho)$ corresponds to a periodic orbit about the origin. For these solutions the energy is given by

$$\mathcal{H}(p) = p^2 - 4.$$

For $\mathcal{H} = \mathcal{H}_1 := \mathcal{H}(p_1)$ the solution to (13) has infinite period. As \mathcal{H} (and therefore p) is reduced, there is a value $\mathcal{H}_2 \in (0, \mathcal{H}_1)$ such that the periodic orbit is hyperbolic for $\mathcal{H} \in (\mathcal{H}_2, \mathcal{H}_1)$ and elliptic for $\mathcal{H} < \mathcal{H}_2$. Moreover, a new solution branch bifurcates from the antidiagonal solution at $\mathcal{H} = \mathcal{H}_2$. The bifurcation diagram is given in Fig. 3 and selected solutions on the bifurcating branch are shown in Fig. 4; the bifurcation at $\mathcal{H} = \mathcal{H}_2$ is label 2 in Fig. 3. Solutions on the new branch connect the zero-velocity surfaces about $(-\pi, \pi)$ and $(\pi, -\pi)$.

Note that the period becomes infinite as $\mathcal{H} \searrow 0$, and at $\mathcal{H} = 0$ the branch seems to be generated by a concatenation of the heteroclinic orbits that con-

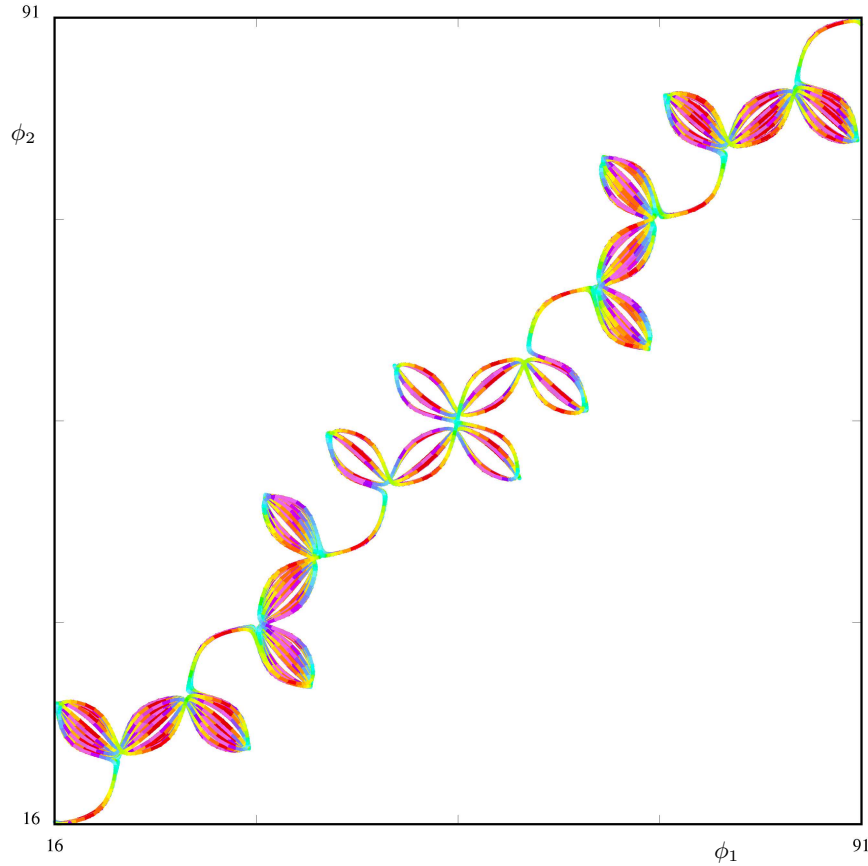


Fig. 5. The long-time integration of certain initial conditions on the zero-energy surface results in an intriguing petal structure. Color indicates the velocity of the solution, where blue/green is slow and red is fast.

nect the zero-velocity surfaces about $(\pm\pi, \mp\pi)$ to the equilibrium point at $(-\pi, -\pi)$.

With further reduction of \mathcal{H} a value $\mathcal{H}_3 \in (0, \mathcal{H}_2)$ is reached (label 3 in Fig. 3) at which a degenerate period-doubling bifurcation occurs. This bifurcation generates a branch of ‘butterfly’-shaped orbits that undergo additional bifurcations and disappear in an infinite-period orbit at $\mathcal{H} = 0$; two of these butterfly-shaped orbits are shown in Fig. 4(a), and further bifurcated orbits are shown in Fig. 4(b). The bifurcation also generates a branch of ‘horseshoe’-shaped orbits that are symmetric about the antidiagonal; see Fig. 4(c) and (d). As we will see, the horseshoes play an important role in the overall dynamics of the system. The horseshoe branch persists through $\mathcal{H} = 0$. There is

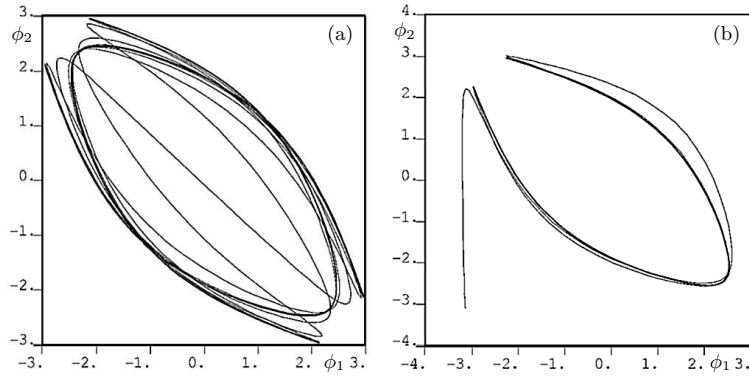


Fig. 6. Heteroclinic orbits in the (ϕ_1, ϕ_2) -plane. Panel (a) shows an orbit in the unstable manifold of the horseshoe orbit for $\gamma = 0.036377$. This orbit connects to the stable manifold of the symmetric partner of the horseshoe orbit. Panel (b) connects the unstable equilibrium $(-\pi, 0, -\pi, 0)$ to the stable manifold of the horseshoe orbit for $\gamma = 0.03638$.

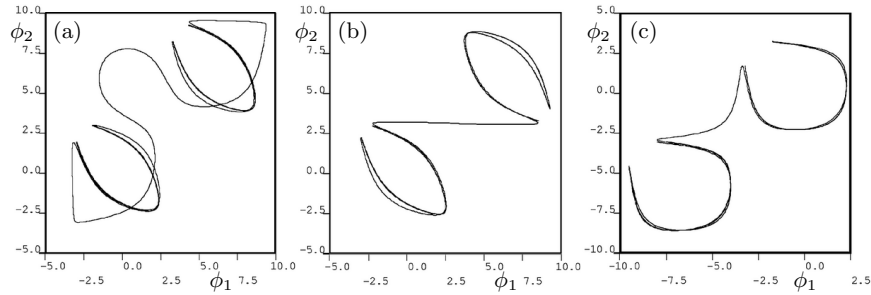


Fig. 7. Connecting orbits between horseshoe orbits in neighboring cells. Here, $(\gamma, \mathcal{H}) = (0.05, 0)$ in panel (a), $(\gamma, \mathcal{H}) = (0.0268297698, 0)$ in panel (b), and $(\gamma, \mathcal{H}) = (0.05, -0.22049)$ in panel (c).

a value $\mathcal{H}_4 < 0$ (label 4 in Fig. 3) at which there is a saddle-node bifurcation leading to a second branch of horseshoes. The second branch ends in an infinite-period orbit at $\mathcal{H} = 0$, where it appears to be the concatenation of three hetero- or homoclinic orbits; two examples are shown in Fig. 4(c). Note that for $\mathcal{H} \in (\mathcal{H}_4, 0)$ there are two distinct branches of horseshoes.

Figure 5 shows the result of a long-time integration in configuration space of system (12) with $\gamma = 0.01$. The trajectory lies on the zero-energy surface and has initial condition

$$\phi_1(0) = -\pi, \quad \dot{\phi}_1(0) = 0, \quad \phi_2(0) = -3.141585,$$

with $\dot{\phi}_2(0)$ determined by the requirement of zero energy. The unbounded trajectory forms an intriguing petal structure. The equilibria where the two

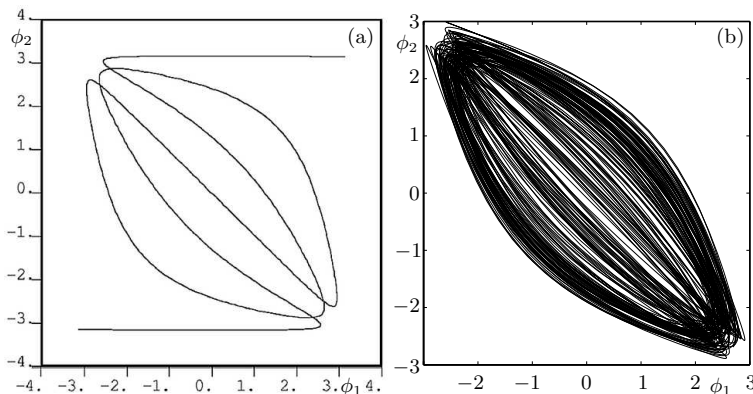


Fig. 8. Solutions to (12) on the zero-energy surface in the (ϕ_1, ϕ_2) -plane. Panel (a) shows a heteroclinic orbit for $\gamma = 0.03638$ that connects the unstable equilibrium $(-\pi, 0, -\pi, 0)$ to its diagonal translate $(\pi, 0, \pi, 0)$. Panel (b) shows a solution integrated for time $T \in [0, 700]$ with $\gamma = 0.01$; the initial condition is $\phi_1(0) = -\phi_2(0) = 2.690233$, and $\dot{\phi}_1(0)$ and $\dot{\phi}_2(0)$ chosen so that the energy is zero.

pendula are in the upright position lie along the diagonal at the base of the ‘petals’. In this motion each pendulum crosses the upright position and changes its direction many times. The petals facing out from the diagonal of the vine-like structure are created when one pendulum crosses the upright position while the other stops and reverses direction. The trajectory moves back and forth along the diagonal in a seemingly erratic fashion. This and similar trajectories are induced by the rich structure of connecting orbits joining the horseshoes and the equilibria, as we now describe briefly.

Figure 6(a) shows a heteroclinic connection between the unstable manifold of the horseshoe orbit for $\gamma = 0.036377$ and the stable manifold of its symmetric partner (i.e., its reflection in the main diagonal). Figure 6(b) shows a heteroclinic orbit that connects the unstable equilibrium $(-\pi, 0, -\pi, 0)$ to the stable manifold of the horseshoe orbit for $\gamma = 0.03638$. Figure 7 shows connections between horseshoes in neighboring cells. Panels (a) and (b) show two solutions in the zero-energy surface, while panel (c) shows a solution for $\mathcal{H} = -0.22049$. Figure 8(a) shows a heteroclinic connection between the unstable equilibrium $(-\pi, 0, -\pi, 0)$ and its diagonal translate $(\pi, 0, \pi, 0)$. These connections provide the escape routes from cell to cell, but not all trajectories are ejected from their initial cells; many are simply trapped inside a horseshoe, as shown in Figure 8(b).

3 Rotations

In addition to equilibria and periodic solutions, system (5) may also have *running solutions* or *k-rotations*. These are solutions for which there exists a time $T > 0$ such that $\phi_j(t + T) = \phi_j(t) + 2k\pi$ for some integer $k \geq 1$. One can anticipate that rotations exist only for the appropriate relationship between the damping and the applied torque in the dissipative case. If we map the configuration space onto a cylinder then these solutions are periodic with period T . To construct a k -rotation we solve the initial value problem for system (6) with

$$s(0) = 0, \quad \dot{s}(0) = p_2, \quad r(0) = p_3, \quad \text{and} \quad \dot{r}(0) = p_4.$$

Solutions depend on the three ‘state’ parameters $\mathbf{p} = (p_2, p_3, p_4)$ and the three ‘system’ parameters ε, γ, I . For simplicity we regard the coupling strength $\gamma > 0$ as fixed and only deal with the two system parameters $\mathbf{q} = (\varepsilon, I)$. A solution to the initial value problem, written in the form

$$[s(t; \mathbf{p}, \mathbf{q}), r(t; \mathbf{p}, \mathbf{q})],$$

is a k -rotation if there exists a minimal $T > 0$ such that

$$\begin{cases} s(T; \mathbf{p}, \mathbf{q}) - 2\pi k = 0 \\ \dot{s}(T; \mathbf{p}, \mathbf{q}) - p_2 = 0, \\ r(T; \mathbf{p}, \mathbf{q}) - p_3 = 0, \\ \dot{r}(T; \mathbf{p}, \mathbf{q}) - p_4 = 0. \end{cases} \quad (14)$$

It is easy to see that in the Hamiltonian case ($\mathbf{q} = \mathbf{0}$) there exist $T_0 > 0$ and state parameters \mathbf{p}_0 such that $[s(t; \mathbf{p}_0, \mathbf{0}), r(t; \mathbf{p}_0, \mathbf{0})]$ is a k -rotation with period T_0 for each $k \geq 1$. We define $\mathcal{P}_0 = (T_0, \mathbf{p}_0, \mathbf{0})$ and say that a continuation of the solution $[s(t; \mathbf{p}_0, \mathbf{0}), r(t; \mathbf{p}_0, \mathbf{0})]$ to a neighborhood of \mathcal{P}_0 is *regular* if there is a distinguished state parameter and a distinguished system parameter such that the remaining state and system parameters are all smooth functions of the distinguished ones in a full neighborhood of \mathcal{P}_0 .

It is an easy consequence of the Implicit Function Theorem that in-phase rotations ($k = 1$) always have a regular continuation. Here, we consider the general case, which is more complicated. The differential of (14) at \mathcal{P}_0 is the matrix

$$\Delta = (\Delta_0 \mid \zeta_\varepsilon \mid \zeta_I),$$

where

$$\Delta_0 = \left[\begin{array}{cccc} \dot{s} & s_{p_2} & s_{p_3} & s_{p_4} \\ \ddot{s} & \dot{s}_{p_2} & \dot{s}_{p_3} & \dot{s}_{p_4} \\ \dot{r} & r_{p_2} & r_{p_3} & r_{p_4} \\ \ddot{r} & \dot{r}_{p_2} & \dot{r}_{p_3} & \dot{r}_{p_4} \end{array} \right] \Big|_{\mathcal{P}_0}, \quad \zeta_\varepsilon = \begin{pmatrix} s_\varepsilon \\ \dot{s}_\varepsilon \\ r_\varepsilon \\ \dot{r}_\varepsilon \end{pmatrix}, \quad \text{and} \quad \zeta_I = \begin{pmatrix} s_I \\ \dot{s}_I \\ r_I \\ \dot{r}_I \end{pmatrix}.$$

Here, Δ_0 is the differential of the Hamiltonian continuation problem, that is, the problem of continuing $(s, r)(\mathcal{P}_0)$ to a neighborhood of \mathcal{P}_0 in the subspace

$\mathbf{q} = \mathbf{0}$. For the Hamiltonian problem, conservation of energy provides a relationship between s , \dot{s} , r , and \dot{r} so that, generically, only three of them are independent, i.e., generically

$$\text{rank}(\Delta_0) = 3. \quad (15)$$

When (15) holds then there is a regular continuation of $(s, r)(\mathcal{P}_0)$ if there exists

$$\zeta^* \in \text{span}\{\zeta_\varepsilon, \zeta_I\} \quad \text{such that} \quad \zeta^* \notin \text{range}(\Delta_0), \quad (16)$$

that is, ζ^* can be chosen such that

$$\text{rank}(\Delta_0 | \zeta^*) = 4.$$

Let $X(t)$ denote the fundamental matrix solution to the variational system associated with (6) at $(s, r)(\mathcal{P}_0)$. As is shown in [3], the differential Δ_0 then becomes

$$\Delta_0 = (\zeta_T | \xi_2 | \xi_3 | \xi_4),$$

where

$$\zeta_T = \left(\begin{array}{c} \dot{s} \\ \ddot{s} \\ \dot{r} \\ \ddot{r} \end{array} \right) \Big|_{\mathcal{P}_0} = \left(\begin{array}{c} p_2^0 \\ 0 \\ p_4^0 \\ -2\gamma p_3^0 - \sin p_3^0 \end{array} \right)$$

and the ξ_j for $j = 2, 3, 4$ are the corresponding columns of $X(T_0) - \text{Id}$. In order to satisfy (15) and (16) there are two possibilities: either

$$\text{rank}(X(T_0) - \text{Id}) = 3 \quad \text{and} \quad \zeta_T \in \text{range}(X(T_0) - \text{Id}) \quad (17)$$

or

$$\text{rank}(X(T_0) - \text{Id}) = 2 \quad \text{and} \quad \zeta_T \notin \text{range}(X(T_0) - \text{Id}). \quad (18)$$

If (17) holds there is no distinguished state parameter and hence no regular continuation. We note that this case was never observed in any of the numerical studies reported in [3]. On the other hand, possibility (18) is known to occur. Suppose (18) holds and let $\{i_1, i_2, i_3\}$ be a permutation of $\{2, 3, 4\}$ such that

$$\text{range}(X(T_0) - \text{Id}) = \text{span}\{\xi_{i_1}, \xi_{i_2}\}.$$

Then there is a Hamiltonian continuation of $(s, r)(\mathcal{P}_0)$ with T , p_{i_1} , and p_{i_2} expressed as smooth functions of p_{i_3} in a neighborhood of $p_{i_3}^0$. If, in addition, (16) holds then there is a regular continuation in a neighborhood of \mathcal{P}_0 .

The choice of distinguished system parameter is arbitrary. Suppose, for instance, that (s, r) is a regular continuation of $(s, r)(t; \mathbf{p}_0, \mathbf{0})$ with distinguished system parameter ε . Then we have a relation of the form $I = H(\cdot, \varepsilon)$, where H is a smooth function. However, k -rotations must satisfy the *kinetic energy relation*

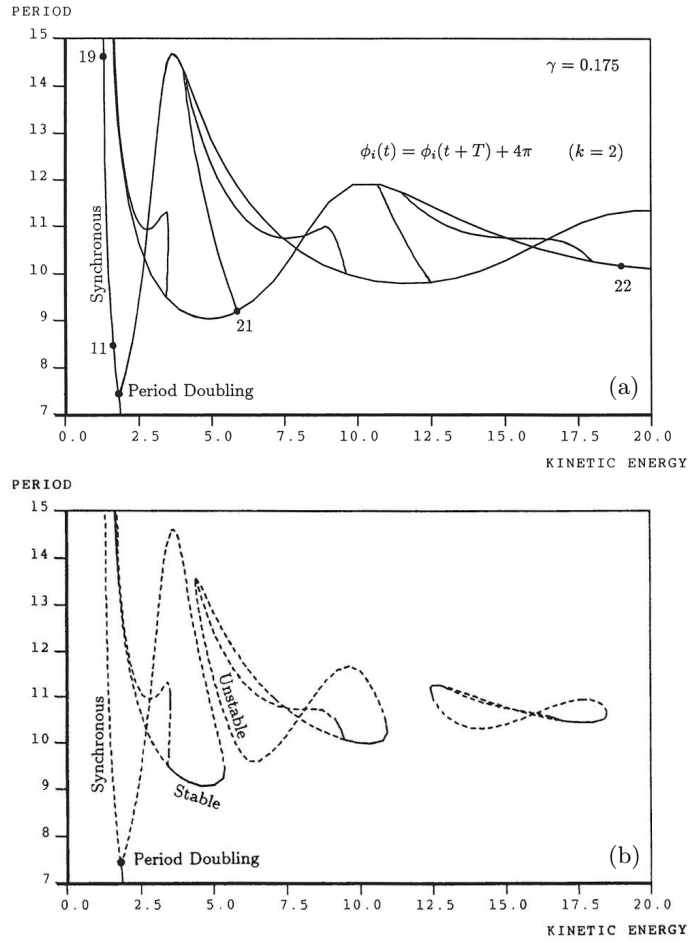


Fig. 9. Solutions of (12) for $\gamma = 0.175$ as a function of the kinetic energy for $I = 0$ (a) and variable I (b). From D.G. Aronson, E.J. Doedel and H.G. Othmer, The dynamics of coupled current-biased Josephson junctions II, *Internat. J. Bifur. Chaos Appl. Sci. Engrg.* 1(1) (1991) 51–66 ©1991, with permission from World Scientific Publishers; reprinted with permission.

$$I = \frac{\varepsilon}{2k\pi} \int_0^T (\dot{s}^2 + \dot{r}^2) dt.$$

It follows that

$$\left. \frac{\partial H}{\partial \varepsilon} \right|_{\mathcal{P}_0} > 0.$$

Therefore, we can invert H to obtain $\varepsilon = h(\cdot, I)$ and we get a regular continuation with I as the distinguished system parameter.

Figure 9(a) shows some branches of 2-rotations with $\mathbf{q} = \mathbf{0}$ and $\gamma = 0.175$; the plot shows the period T versus the kinetic energy. Figure 9(b) shows the equivalent solutions for $\mathbf{q} = (0.01, I)$ with I variable. The bifurcation at label 21 in Fig. 9(a) does not persist as ε is increased since there is a regular continuation at this point. The bifurcations to the right of label 21 do persist, because condition (16) fails in this case.

4 Stability and bifurcations of the in-phase rotations

Most of the solution branches shown in Fig. 9(a) are 2-rotations for the Hamiltonian system. The exception is the left-most branch of synchronous or in-phase rotations. Here we investigate the stability and bifurcation properties of these solutions and their extensions to the damped/driven regime. To simplify the analysis we scale the damping ε and the torque I together by assuming that $I = \varepsilon A$ for some fixed $A > 0$. It is clear that system (5) has a one-parameter family of rotations $\Omega_\tau(\varepsilon)$ defined by $\phi_1(t) = \phi(t)$ and $\phi_2(t) = \phi(t + \tau)$ for each $\tau \in \mathbb{R}$ when $\gamma = 0$. It was shown in [5] that the only member of this family that can be continued for $\gamma \neq 0$ is the in-phase rotation $\Omega_0(\varepsilon)$. In this section we discuss the stability of $\Omega_0(\varepsilon)$ as the parameters ε and γ are varied.

It is known that for fixed $A > 4/\pi$ and each $\varepsilon > 0$, the equation

$$\ddot{\phi} + \sin \phi = \varepsilon(A - \dot{\phi}) \quad (19)$$

has a unique rotation solution for which $\dot{\phi} > 0$ [12]. If we translate time so that $\phi(0) = 0$ then there is a unique positive $\xi(\varepsilon) > 2$ such that the rotation solution satisfies $\dot{\phi}(0) = \xi(\varepsilon)$. As $\varepsilon \rightarrow 0$, we have $\xi(\varepsilon) \rightarrow \xi_0$, where $\xi_0 = \xi_0(A) > 2$ is the unique solution of

$$2\pi A = \int_0^{2\pi} \sqrt{\xi^2 - 2 + 2 \cos \theta} d\theta.$$

Note that ξ_0 can have any value in the interval $(2, \infty)$ depending on the choice of $A > 4/\pi$. We denote the rotation solution by $\phi^*(\varepsilon)$ and its period by $T^*(\varepsilon)$.

In order to determine the stability of the in-phase rotation $\phi^*(\varepsilon)$ we must find the associated Floquet multipliers, which are the eigenvalues at $t = T^*(\varepsilon)$ of the fundamental matrix solution to the variational system associated with (6) at $\phi^*(\varepsilon)$. For this purpose it is convenient to order the variables as (r, u, s, v) . Then we have to solve the system

$$\dot{V} = \begin{bmatrix} 0 & 1 & 0 & 0 \\ -\cos \phi^*(\varepsilon) - 2\gamma & -\varepsilon & 0 & 0 \\ 0 & 0 & 0 & 1 \\ 0 & 0 & -\cos \phi^*(\varepsilon) & -\varepsilon \end{bmatrix} V \quad (20)$$

subject to the initial condition $V(0) = \text{Id}$. System (20) decomposes into the two 2×2 subsystems

$$\dot{X} = \begin{bmatrix} 0 & 1 \\ -\cos \phi^*(\varepsilon) - 2\gamma & -\varepsilon \end{bmatrix} X, \quad X(0) = \text{Id} \quad (21)$$

and

$$\dot{Y} = \begin{bmatrix} 0 & 1 \\ -\cos \phi^*(\varepsilon) & -\varepsilon \end{bmatrix} Y, \quad Y(0) = \text{Id}. \quad (22)$$

Subsystem (22) determines stability with respect to the in-phase subspace and subsystem (21) determines stability with respect to the orthogonal complement of this subspace. It is easy to see that $Y = (\dot{\phi}, \ddot{\phi})^T$ is a $T^*(\varepsilon)$ -periodic solution of (22). Therefore, the Floquet multipliers associated with subsystem (22) are 1 and $\exp(-\varepsilon T^*(\varepsilon))$, regardless of the value of γ . Thus, to determine the stability of $\phi^*(\varepsilon)$ it suffices to study the 2×2 system (21).

Let $\Psi(t, \gamma, \varepsilon)$ denote the fundamental matrix solution to (21). Then the Floquet multipliers are the eigenvalues of $\Psi(T^*(\varepsilon), \gamma, \varepsilon)$, that is, the roots of

$$\lambda^2 - \Theta(\gamma, \varepsilon)\lambda + \exp(-\varepsilon T^*(\varepsilon)) = 0,$$

where

$$\Theta(\gamma, \varepsilon) = \text{trace}(\Psi(T^*(\varepsilon), \gamma, \varepsilon)).$$

Therefore, the multipliers are

$$\lambda^\pm = \frac{1}{2} \left(\Theta \pm \sqrt{\Theta^2 - 4 \exp(-\varepsilon T^*(\varepsilon))} \right),$$

and it follows that $\phi^*(\varepsilon)$ is stable if $|\Theta| < 1 + \exp(-\varepsilon T^*(\varepsilon))$ and unstable if $|\Theta| > 1 + \exp(-\varepsilon T^*(\varepsilon))$.

When $\varepsilon \rightarrow 0$, the second-order equation associated with system (21) reduces to a Hill's equation

$$\ddot{x} + (2\gamma - q(t))x = 0, \quad (23)$$

where the potential is given by

$$q(t) = -\cos \phi^*(\varepsilon)(t)|_{\varepsilon=0}. \quad (24)$$

Moreover,

$$\Theta(\gamma, \varepsilon) \rightarrow \Theta_0(\gamma) = \left(\psi_1(T_0) + \dot{\psi}_2(T_0) \right),$$

where ψ_1 and ψ_2 are solutions to (17) that satisfy $\psi_1(0) = \dot{\psi}_2(0) = 1$ and $\dot{\psi}_1(0) = \psi_2(0) = 0$, and $T_0 = T^*(0)$.

The general theory for Hill's equation [11] shows that there exists a sequence of eigenvalues

$$-\infty < \gamma_0 < \gamma_1 \leq \gamma_2 < \gamma_3 \leq \gamma_4 < \dots$$

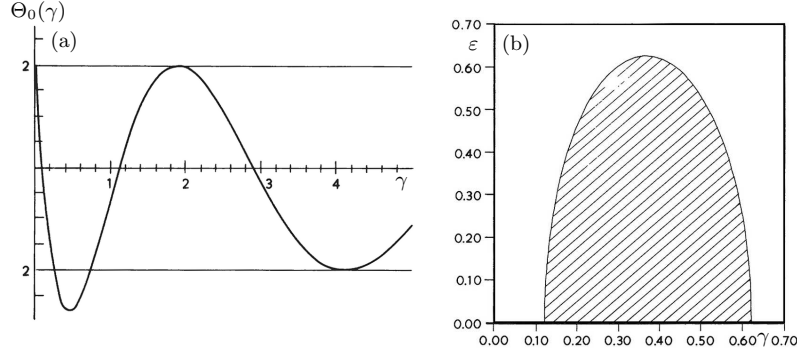


Fig. 10. The graph of $\Theta_0(\gamma)$ (a) and the locus of period-doubling bifurcations from $\phi^*(\varepsilon)$ for $A = 5/3$ (b). The in-phase rotation is unstable in the hatched region. From E.J. Doedel, D.G. Aronson and H.G. Othmer, The dynamics of coupled current-biased Josephson junctions I, *IEEE Trans. Circ. Sys.* 35(7) (1988) 810–817 ©1988 by IEEE; reprinted with permission.

with $\gamma_j \rightarrow \infty$ as $j \rightarrow \infty$, such that

$$\begin{aligned}
 |\Theta_0| < 2 \text{ and } \dot{\Theta}_0 < 0 & \text{ on } (\gamma_0, \gamma_1) \cup (\gamma_4, \gamma_5) \cup \dots, \\
 |\Theta_0| < 2 \text{ and } \dot{\Theta}_0 > 0 & \text{ on } (\gamma_2, \gamma_3) \cup (\gamma_6, \gamma_7) \cup \dots, \\
 \Theta_0 > 2 & \text{ on } (-\infty, \gamma_0) \cup (\gamma_3, \gamma_4) \cup (\gamma_7, \gamma_8) \cup \dots, \\
 \Theta_0 < -2 & \text{ on } (\gamma_1, \gamma_2) \cup (\gamma_5, \gamma_6) \cup \dots.
 \end{aligned} \tag{25}$$

At $\gamma = 0$ system (21) reduces to (22), which has a T_0 -periodic solution. Thus, 0 is an eigenvalue of (23) with T_0 -periodic boundary conditions, and we know from previous remarks that the associated eigenfunction is strictly positive. It follows from Sturm-Liouville theory that 0 is the smallest eigenvalue for this problem and, therefore, $\gamma_0 = 0$. Consequently, $\Theta_0(\gamma) > 2$ for all $\gamma < 0$.

According to Goldberg's theorem [7], equation (23) has exactly one finite interval of instability if and only if the potential q is periodic and integrable, and satisfies

$$\ddot{q} = 3q^2 + \alpha q + \beta \tag{26}$$

for some constants α and β , that is, if and only if q is an elliptic function. In the present case, since $\phi^*(0)$ is a rotation it follows from (24) that q is periodic. Moreover, using (19) with $\varepsilon = 0$ and its first integral, one can verify that (26) is satisfied. Thus, there is precisely one finite interval of instability for $\gamma > 0$, and the numerical computations performed in [5] show that this interval is (γ_1, γ_2) . It follows that $\gamma_{2j-1} = \gamma_{2j}$ for all $j > 2$ and that $|\Theta_0(\gamma)| = 2$ for $\gamma = \gamma_{2j}$ with $j > 1$. The graph of $\Theta_0(\gamma)$ is shown in Fig. 10(a).

The second-order equation corresponding to (21) is

$$\ddot{x} + \varepsilon \dot{x} + (2\gamma + \cos \phi^*(\varepsilon))x = 0. \tag{27}$$

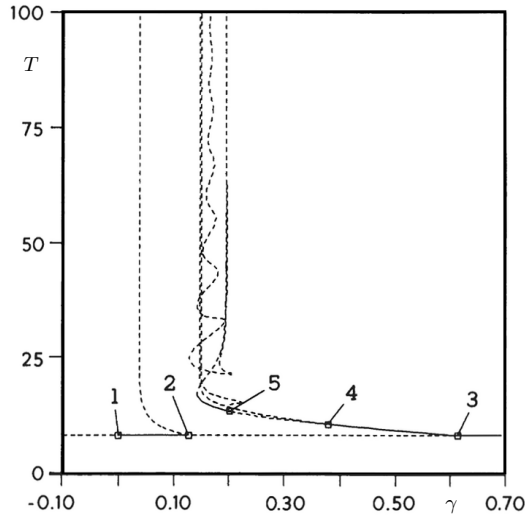


Fig. 11. The bifurcation diagram for (6), represented as the period T versus γ for $A = 5/3$. From E.J. Doedel, D.G. Aronson and H.G. Othmer, The dynamics of coupled current-biased Josephson junctions I, *IEEE Trans. Circ. Sys.* 35(7) (1988) 810–817 ©1988 by IEEE; reprinted with permission.

If $\gamma = 0$ then $x_1(t) = \dot{\phi}^*(\varepsilon)(t)$ is a strictly positive $T^*(\varepsilon)$ -periodic solution to (27) for any $\varepsilon > 0$. Thus, $\gamma = 0$ is an eigenvalue of (27) for any $\varepsilon > 0$, and it is a simple eigenvalue because

$$x_2(t) = \dot{\phi}^*(\varepsilon)(t) \int_0^t \frac{e^{-\varepsilon\tau}}{[\dot{\phi}^*(\varepsilon)(\tau)]^2} d\tau$$

is a linearly independent non-periodic solution. Using these solutions one can construct the fundamental matrix solution to (21) and show that $\Theta_\gamma(0, \varepsilon) < 0$. It follows that the infinite instability interval $(-\infty, 0)$ remains invariant for $\varepsilon > 0$ and that $\dot{\phi}^*(\varepsilon)$ becomes stable as γ increases through 0. Numerical computations show that there is a ‘vertical’ bifurcation from $\dot{\phi}^*(\varepsilon)$ at $\gamma = 0$; the numerical results are described in more detail below.

By continuity, the unique instability interval (γ_1, γ_2) for $\varepsilon = 0$ persists for sufficiently small $\varepsilon > 0$. The numerical computations done in [5] strongly suggest that the remaining eigenvalues γ_{2j} disappear for $\varepsilon > 0$. Consequently, for sufficiently small $\varepsilon > 0$ the rotation solution $\dot{\phi}^*(\varepsilon)$ is unstable for $\lambda \in (-\infty, 0) \cup (\gamma_1(\varepsilon), \gamma_2(\varepsilon))$ and stable otherwise. Furthermore, there exists $\tilde{\varepsilon} = \tilde{\varepsilon}(A) > 0$ such that $\gamma_1(\tilde{\varepsilon}) = \gamma_2(\tilde{\varepsilon})$, and $\dot{\phi}^*(\varepsilon)$ is unstable on \mathbb{R}^- and asymptotically stable on \mathbb{R}^+ whenever $\varepsilon > \tilde{\varepsilon}$; see Fig. 10. Note that the bifurcations at $\gamma = \gamma_j(\varepsilon)$, $j = 1, 2$, are period-doubling bifurcations, because the multiplier passes through -1 ; see Fig. 10(b). In the Hamiltonian case these two bifurcations project onto the point labeled ‘Period Doubling’ in Fig. 9(a).

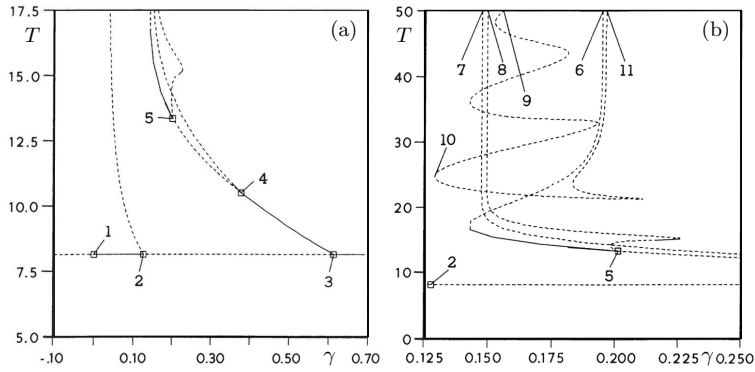


Fig. 12. Details of the bifurcation diagram shown in Fig. 11. The points in panel (a) labeled 1, 4, and 5 are transcritical bifurcations, while those labeled 2 and 3 are period-doubling bifurcations. There are two regions of stability along the asynchronous branch that bifurcates at label 3. Panel (b) shows a blow-up of the region around label 5 in panel (a). From E.J. Doedel, D.G. Aronson and H.G. Othmer, *The dynamics of coupled current-biased Josephson junctions I*, *IEEE Trans. Circ. Sys.* 35(7) (1988) 810–817 ©1988 by IEEE; reprinted with permission.

We now discuss the numerically computed bifurcation behavior in the interval (γ_1, γ_2) for the value $\varepsilon = \varepsilon^* = 0.15$ used in [10]. Then the period-doubling bifurcations from $\phi^*(\varepsilon)$ are at $\gamma_1 = 0.1275$ and $\gamma_2 = 0.6132$. Solution branches that bifurcate from $\phi^*(\varepsilon^*)$ at $\gamma = \gamma_1$ and $\gamma = \gamma_2$ are shown in Fig. 11 with enlarged views given in Fig. 12. Rotations that correspond to some of the labels in Fig. 12 are shown in Fig. 13.

All rotations in Figs. 11 and 12 have winding number 2, so that $\phi_i(T) - \phi_i(0) = 4\pi$, where T is the integration time. The bifurcating branches then connect continuously to the horizontal branch $\phi^*(\varepsilon^*)$. The solutions with labels 2 and 3 in Fig. 12(a) denote the two period-doubling bifurcations from $\phi^*(\varepsilon^*)$. The branch that emanates from label 2 terminates at an orbit of infinite period. The same holds for the branch that emanates from label 3. The solution with label 6 in Fig. 12(b) can be thought of as an approximation to the infinite-period orbit that terminates the branch; it is shown in Fig. 13(a). The infinite-period orbit is a ‘double homoclinic loop’, i.e., an orbit that passes through the same saddle point twice. Note that this branch contains two regions of stable rotations. The solutions with labels 4 and 5 in Fig. 12(a) are secondary transcritical bifurcations, not period-doubling bifurcations. The bifurcating tertiary branches from labels 4 and 5 also terminate in infinite-period orbits past the solutions labeled 7 and 8, respectively; compare Figs. 13(b) and (c). These branches also contain stable portions and further bifurcations that are not shown in Figs. 11 and 12.

The ‘oscillating’ branch of solutions in Fig. 11 is shown in a blow-up in Fig. 12(b); it contains the solutions labeled 9, 10, and 11, which are plot-

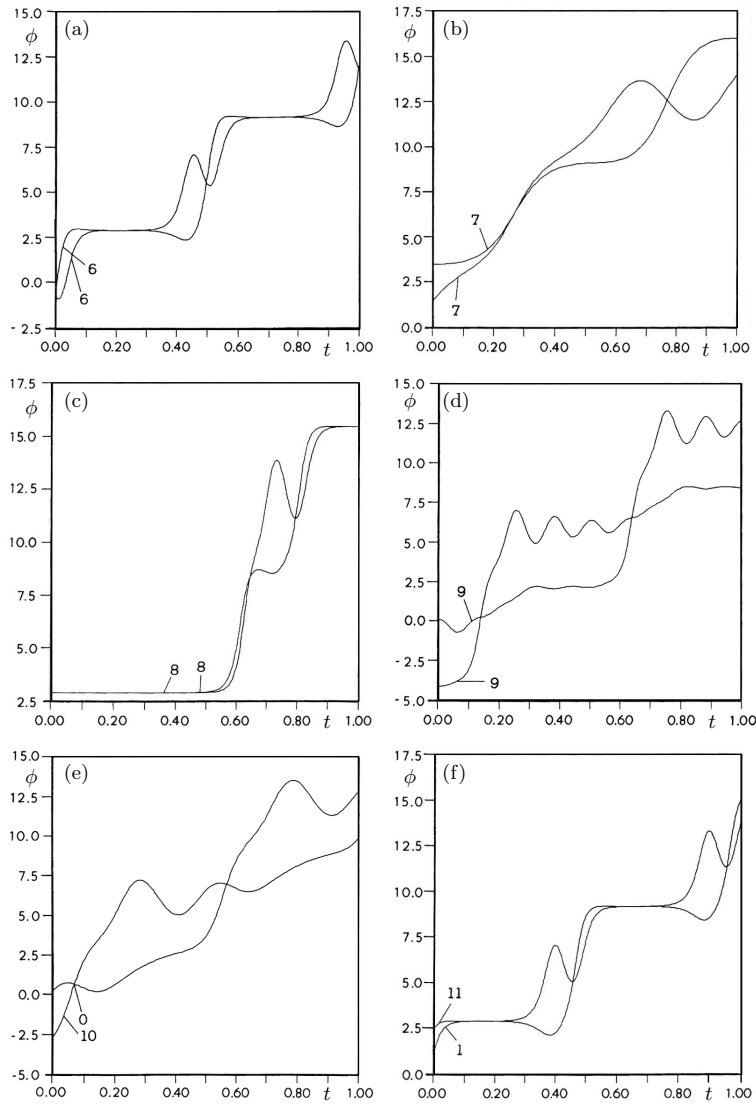


Fig. 13. Some rotations corresponding to the labels in Fig. 12. From E.J. Doedel, D.G. Aronson and H.G. Othmer, The dynamics of coupled current-biased Josephson junctions I, *IEEE Trans. Circ. Sys.* 35(7) (1988) 810–817 ©1988 by IEEE; reprinted with permission.

ted in Figs. 13(d), (e), and (f), respectively. This branch terminates in an infinite-period orbit at both end points of the γ interval in which it exists. The solutions with labels 9 and 11 can be considered as approximations to these orbits. Solution 9 approximates an infinite-period orbit containing two distinct

unstable equilibria, each of which has one complex conjugate pair of eigenvalues; see Fig. 13(d). Solution 11, at the other end of the branch, is a double homoclinic loop; see Fig. 13(f). Along this branch there are small intervals of stable behavior near the limit points. For example, one such stable interval is near the solution with label 10 on the lower part of the branch. These stable regions are so small that they cannot be distinguished in Fig. 12(b). They are bounded by bifurcations that lead to more complicated solution types. Many of these more complicated, stable solutions can be observed numerically by careful choice of initial data and accurate integration. For example, a stable rotation such as solution 10 in Fig. 13(e) can be obtained by accurately choosing initial data near solution 10 in Fig. 12(b), on the small portion of the branch that consists of stable rotations.

5 Conclusions

We presented an overview of the dynamics of a model of a ring of superconducting material that contains two Josephson junctions, which is known as a SQUID. The resulting system equations are identical (in non-dimensional form) to the equations modeling two pendula that are coupled by a linear torsional spring or bar and forced with an applied torque. Our analysis involved intensive use of AUTO to construct bifurcation diagrams and rotating solutions that can only be found explicitly for the Hamiltonian case.

A complex bifurcation structure organizes the existence of rotation solutions. We focused particularly on the case of fixed coupling parameter γ and varying damping coefficient ε and forcing I . We found the conditions under which in-phase rotation solutions that exist for $\varepsilon = 0$ persist; the resulting branch leads to a series of bifurcating branches. In particular, there is a region of relatively small values of γ and ε in which the in-phase rotation is unstable.

Maginu [10] was the first to observe the instability for intermediate values of γ and suitable ε and I . His numerical studies indicate the presence of chaos in the unstable range. The results discussed here provide a more detailed, though still incomplete, understanding of the transitions in dynamics suggested in [10].

Acknowledgments

We thank Sebius Doedel, John Guckenheimer and Björn Sandstede for their contributions during our collaboration on the material in this chapter. Furthermore, we are grateful to World Scientific Publishers and IEEE for permission to reproduce previously published material from [3] and from [5], respectively.

References

1. E. Altshuler and R. Garcia. Josephson junctions in a magnetic field: Insights from coupled pendula. *Am. J. Phys.*, 71(4): 405–408, 2003.
2. D. G. Aronson, E. J. Doedel, J. Guckenheimer, A. Jorba, and B. Sandstede. On the dynamics of torsion-coupled pendula. Unpublished, 2002.
3. D. G. Aronson, E. J. Doedel, and H. G. Othmer. The dynamics of coupled current-biased Josephson junctions II. *Internat. J. Bifur. Chaos Appl. Sci. Engrg.*, 1(1): 51–66, 1991.
4. V. N. Belykh, N. F. Pedersen, and O. H. Soerensen. Shunted-Josephson-junction model. II. The nonautonomous case. *Physical Review B*, 16(11): 4860–71, 1977.
5. E. J. Doedel, D. G. Aronson, and H. G. Othmer. The dynamics of coupled current-biased Josephson junctions I. *IEEE Trans. Circ. Sys.*, 35(7): 810–817, 1988.
6. L. Finger. The Josephson junction circuit family: Network theory. *Int. J. Circ. Th. Appl.*, 28(4): 371–420, 2000.
7. W. Goldberg. Necessary and sufficient conditions for determining a Hill’s equation from its spectrum. *J. Math. Anal. Appl.*, 55: 549–554, 1976.
8. B. D. Josephson. Supercurrents through barriers. *Phys Letts*, 1: 201, 1962.
9. Konstantin K. Likharev. *Dynamics of Josephson Junctions and Circuits*. Gordon and Breach Publishers, New York, 1986.
10. K. Maginu. Spatially homogeneous and inhomogeneous oscillations and chaotic motion in the active Josephson junction line. *SIAM J. Appl. Math.*, 43(2): 225–243, 1983.
11. W. Magnus and S. Winkler. *Hill’s Equation*. Dover Publ., New York, 1979.
12. N. Minorsky. *Nonlinear Oscillations*. Robert E. Krieger Publishing Co., Malabar, Fla., 1983.
13. F. M. A. Salam and S. S. Sastry. The complete dynamics of the forced Josephson junction circuit: the regions of chaos. In J. Chandra, editor, *Chaos in Nonlinear Dynamical Systems*, pages 43–55. SIAM, Philadelphia, 1984.